Dynamics on the Laminar-Turbulent Boundary and the Origin of the Maximum Drag Reduction Asymptote

Dynamics on the Laminar-Turbulent Boundary and the Origin of the Maximum Drag Reduction Asymptote

Li Xi[1] and Michael D. Graham[2,*]

[1]Department of Chemical Engineering, Massachusetts Institute of Technology, Cambridge, Massachusetts 02142, USA
[2]Department of Chemical and Biological Engineering, University of Wisconsin-Madison, Madison, Wisconsin 53706, USA

(Received 28 July 2011; published 11 January 2012)

Dynamical trajectories on the boundary in state space between laminar and turbulent plane channel flow—edge states—are computed for Newtonian and viscoelastic fluids. Viscoelasticity has a negligible effect on the properties of these solutions, and, at least at a low Reynolds number, their mean velocity profiles correspond closely to experimental observations for polymer solutions in the maximum drag reduction regime. These results confirm the existence of weak turbulence states that cannot be suppressed by polymer additives, explaining the fact that there is an upper limit for polymer-induced drag reduction.

DOI: 10.1103/PhysRevLett.108.028301 PACS numbers: 83.60.Yz, 47.27.ed, 47.27.N-, 47.57.Ng

When flow in a pipe or channel turns turbulent, its frictional resistance increases abruptly. Introducing long-chain polymer additives can significantly reduce this resistance [1–3]. This polymer drag reduction (DR) effect saturates at high levels of viscoelasticity: an asymptotic upper limit is reached that is insensitive to polymer concentration, molecular weight or chemical structure. In this limit, mean velocity profiles $U_m(y)$ under different conditions collapse onto the log-law relationship reported by Virk: $U_m^+ = 11.7\ln y^+ - 17.0$ [1]. (The superscript "+" denotes quantities nondimensionalized in inner velocity and length scales $\sqrt{\tau_w/\rho}$ and $\eta/\sqrt{\rho\tau_w}$: τ_w is the time- and area-averaged wall shear stress, η and ρ are the fluid viscosity and density, and y is the distance from the wall.) This so-called maximum drag reduction (MDR) phenomenon remains the most important unsolved problem in viscoelastic turbulence. Additionally, it has long been hoped that understanding drag reduction in polymer solutions might lead to new insights into how to reduce energy consumption in Newtonian fluids as well.

Recent studies [4,5] revealed that in both Newtonian and viscoelastic flows, the turbulent self-sustaining process exhibits distinct phases in its dynamics. In the Newtonian limit, so-called active turbulence dominates, where the flow structures show strong vortices and wavy streaks. On rare occasions, intervals with weak turbulence activity show up: flow structures during these hibernating turbulence intervals resemble MDR turbulence, showing features [6–8] such as weak streamwise vortices, almost streamwise-invariant streaks and an instantaneous mean velocity profile that approaches the Virk log-law profile. With increasing viscoelasticity, active intervals are shortened while hibernating intervals are virtually unaffected. Accordingly, hibernation occurs more frequently, leading to flows increasingly similar to MDR. Related results have recently been found in boundary layer flow [9]. These results indicate that MDR might be associated with a type of weak turbulence already existing in Newtonian flow that only becomes unmasked at a high level of viscoelasticity as suggested by [2]. Furthermore, the dynamics of hibernating turbulence are consistent with suggestions that turbulence in the MDR regime is somehow "transitional" [3,9,10] or "marginal" [11].

In a well-defined sense, the weakest, most marginal form of self-sustaining turbulence is a flow that asymptotically in time approaches neither the turbulent state nor the laminar state—an edge state [12–14]. An edge state lies on an invariant surface in state space that is a generalization of a basin boundary between two attractors to the situation where one attractor might be replaced by a very long-lived transient; there is evidence that this is the situation with turbulence in some cases [15]. Lebovitz [14] calls such a surface a "weak" basin boundary. Initial conditions starting on one side of the edge surface develop into turbulence, those on the other side directly decay to laminar flow, and initial conditions on the surface itself remain on the surface, asymptotically approaching an edge state. As such, edge states are saddle structures in state space. These states have attracted much recent attention [12,16–18]. Past studies have focused on laminar-turbulent transition in Newtonian flows. In the present study, we focus on the connection between the edge and drag reduction by polymers. In particular, we address two key questions: (1) How does viscoelasticity affect the edge? (2) Is there any similarity between the edge and MDR?

We study plane Poiseuille flow at fixed pressure drop. The x, y, and z coordinates are aligned with the streamwise, wall-normal and spanwise directions, respectively. No-slip boundary conditions apply at the walls and periodic boundary conditions apply in x and z; the periods in these directions are denoted L_x and L_z. The governing equations are

$$\frac{D\mathbf{v}}{Dt} = -\nabla p + \frac{\beta}{\mathrm{Re}}\nabla^2\mathbf{v} + \frac{2(1-\beta)}{\mathrm{Re\,Wi}}\frac{b+5}{b}(\nabla\cdot\boldsymbol{\tau}_p), \quad (1)$$

$$\nabla \cdot \mathbf{v} = 0, \tag{2}$$

$$\frac{\mathrm{Wi}}{2}\left(\frac{D\boldsymbol{\alpha}}{Dt} - \boldsymbol{\alpha}\cdot\nabla\mathbf{v} - (\boldsymbol{\alpha}\cdot\nabla\mathbf{v})^{\mathrm{T}}\right) = -\boldsymbol{\tau}_p, \tag{3}$$

$$\boldsymbol{\tau}_p = \left(\frac{\boldsymbol{\alpha}}{1 - \frac{\mathrm{tr}\,(\boldsymbol{\alpha})}{b}} - \frac{b}{b+2}\boldsymbol{\delta}\right). \tag{4}$$

Here (1) and (2) are conservation of momentum and mass. The polymer contribution is captured by the FENE-P constitutive equation [(3) and (4)] [19]: $\boldsymbol{\tau}_p$ is the polymer stress and $\boldsymbol{\alpha}$ is the polymer conformation tensor. Velocities and lengths are scaled with Newtonian laminar centerline velocity U and half-channel height l. Time t is scaled with l/U and pressure p with ρU^2. Reynolds number $\mathrm{Re} \equiv \rho U l/\eta$ (where η is the total zero-shear viscosity), Weissenberg number $\mathrm{Wi} \equiv 2\lambda U/l$ (λ is the polymer relaxation time), viscosity ratio $\beta \equiv \eta_s/\eta$ (η_s is the solvent viscosity), and b is the polymer extensibility: $\max(\mathrm{tr}(\boldsymbol{\alpha})) < b$. Stress is scaled with the shear modulus in the limit $b \to \infty$. All results are obtained with box size $(L_x^+, L_z^+) = (720, 140)$; time steps are $\delta t = 0.02$ for $\mathrm{Re} = 3600$ (friction Reynolds number $\mathrm{Re}_\tau = \sqrt{2\,\mathrm{Re}} = 84.85$) and $\delta t = 0.01$ for $\mathrm{Re} = 14\,400$; for viscoelastic runs $\beta = 0.97$ and $b = 5000$. Additional details are reported elsewhere [20].

To compute edge states, we follow the same method as previous studies [12,18]. Using any point in the state space as the initial condition, a short direct numerical simulation (DNS) will tell which side of the edge surface it belongs to: if a strong turbulent burst is found the point is on the turbulent side; if the solution decays directly to the laminar state it is on the laminar side. Given two points on opposite sides of the edge surface, denoted $\mathbf{v}_{T0}$ and $\mathbf{v}_{L0}$, a line connecting them in the state space $\mathbf{v}(\theta) = \theta\mathbf{v}_{T0} + (1-\theta)\mathbf{v}_{L0}$ must intersect the edge at least once. Therefore through repeated bisection, one can always find a pair of points $\mathbf{v}(\theta_T)$ and $\mathbf{v}(\theta_L)$ that are arbitrarily close to each other, yet located on opposite sides of the edge. In this case both points are sufficiently close to the edge that dynamical trajectories starting from them will stay close to the edge for a long time before diverging from one another. A next round of bisections is then started using a new pair $\mathbf{v}_{T0}$ and $\mathbf{v}_{L0}$ taken from trajectories of the previous round. This process is repeated and the solutions from each iteration are concatenated to form an approximation to a trajectory on the edge. In this study each round of bisection is stopped when $\theta_T - \theta_L \le 10^{-8}$; a new round is started when the bulk-average turbulent kinetic energy differs by a magnitude of 10^{-6}–10^{-5} between the trajectories. Computations are continued until the results are statistically stationary.

A time series of area-averaged wall shear rate $\langle \partial u_x/\partial y\rangle_w$ for a viscoelastic edge state at $\mathrm{Re} = 3600$, $\mathrm{Wi} = 28$ is shown in Fig. 1. Strong asymmetry across the channel center is observed in all our solutions; we have plotted the wall shear rate at the side with stronger velocity fluctuations. Trajectories on the edge are much less chaotic than regular turbulence (cf. [4,5,20]). Intervals with high $\langle \partial u_x/\partial y\rangle_w$ and large temporal variation alternate with those with low $\langle \partial u_x/\partial y\rangle_w$ and almost nonexistent variation. The Newtonian case is very similar, although the average interval between successive peaks is shorter. Variations in the bulk (volume-averaged) $\mathrm{tr}(\boldsymbol{\alpha})$ are also shown in Fig. 1; they are in phase with those of $\langle \partial u_x/\partial y\rangle_w$.

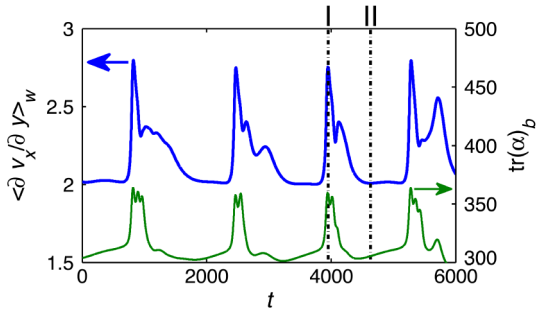

FIG. 1 (color online). Time series of an edge trajectory at $\mathrm{Re} = 3600$, $\mathrm{Wi} = 28$. Thick lines: area-averaged wall shear rate; thin lines: bulk-average $\mathrm{tr}(\boldsymbol{\alpha})$.

Asymmetry of flow structures is clearly reflected in the Reynolds shear stress profiles [Fig. 2(a)]. Therefore, in presenting results, we will define the y axis so that the wall nearest the more substantial dynamics is at $y^+ = 0$. These profiles are all significantly lower in magnitude than regular turbulence, which has a maximum of ≈ 0.6 [5,20]. The Newtonian $\mathrm{Re} = 3600$ profile is even smaller compared with magnitudes within hibernating turbulence. Note that the smallness of Reynolds shear stress is among the major observations during MDR [8,21–23]. An edge solution for $\mathrm{Re} = 14\,400$ has also been computed, and strong asymmetry is also observed. In addition to the primary peak found at $y^+ \approx 35$, where the $\mathrm{Re} = 3600$ profile

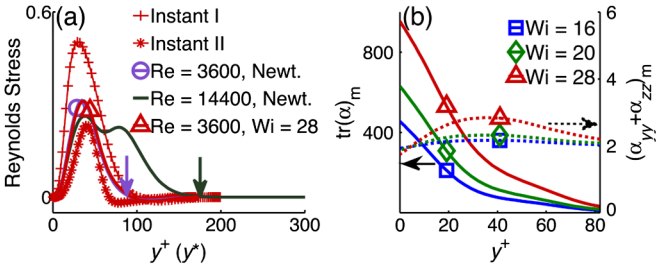

FIG. 2 (color online). (a) Reynolds shear stress profiles. Lines with markers + and ∗ are instantaneous profiles for instants (I) and (II) in Fig. 1(b), scaled in ∗ units; others are time averages, scaled in + units. Arrows mark the positions of the channel centers for the Newtonian time-average profiles. (b) Polymer conformation profiles($\mathrm{Re} = 3600$). Solid lines and left ordinate: mean (area- and time-averaged) profiles of $\mathrm{tr}(\boldsymbol{\alpha})$; dashed lines and right ordinate: mean $\alpha_{yy} + \alpha_{zz}$.

reaches a maximum, a secondary peak is found at $y^+ \approx 75$, indicating nontrivial structure further from the wall than in the Re = 3600 case. The viscoelastic result at Re = 3600 and Wi = 28 is also plotted; it almost collapses onto the corresponding Newtonian profile. Note that for the same Re, β and b, the onset Wi for DR found in an earlier study (focusing on dynamics in the turbulence basin) is ≈ 10 [5]; at Wi = 28, viscoelasticity is strong enough to cause not only substantial DR, but also qualitative changes in flow statistics and structures [5,20]. It is striking that the same level of viscoelasticity does not affect the results on the edge.

Instantaneous profiles of Reynolds shear stress are also shown in Fig. 2(a), for two instants selected from the edge solution at Wi = 28, as marked in Fig. 1. These are nondimensionalized in inner scales based on instantaneous wall shear stress τ_w^* (instead of its time average τ_w); correspondingly, superscript $*$ is used instead of $+$. Instant (I) is taken near a peak of $\langle \partial v_x/\partial y \rangle_w$; here we also observe a much higher $-\langle v_x'^+ v_y'^+ \rangle$ magnitude than instant (II), which is taken in the phase with lower $\langle \partial v_x/\partial y \rangle_w$.

Flow fields for these instants are shown in Fig. 3. Instant (I), which has stronger turbulent activity, shows a shorter characteristic wavelength in the z direction than instant (II). Low- and high-speed streaks have weak dependence in the x direction in both instants [Figs. 3(a) and 3(b)]. At (I) some variation is still observed, which however occurs over a much longer wavelength than in active turbulence (typically ≈ 300 [4,5,20]); at (II) variation along the x axis is barely noticeable. The presence of streamwise vortices is apparent from the structure of the streamwise velocity components. At instant (I) these vortices have similar strength as those in hibernating turbulence, which are a few times weaker than in active turbulence; at instant (II), their strength is an order of magnitude weaker than at (I). Extremely weak vortices and nearly streamwise-invariant streaks are observed in both MDR [6–8] and hibernating turbulence [4,5].

Mean velocity profiles for these two instants as well as time-averaged profiles are plotted in Fig. 4. The profile of instant (II) is slightly above the Virk MDR asymptote, also shown on the plot, while that of (I) is well below; consequently the time-average profile for Re = 3600 and Wi = 28 is remarkably close to it. Comparing time-average profiles for all Re = 3600 cases, we see that viscoelasticity has virtually no effect on the mean velocity: Newtonian and viscoelastic profiles from different Wi overlap one another very closely and are thus difficult to distinguish on the plot. Recall from Fig. 2(a) that insensitivity to viscoelasticity is also found in Reynolds shear stress.

The origin of the insensitivity of edge solution to viscoelasticity is seen upon examination of the polymer conformation profiles, Fig. 2(b). Although tr($\boldsymbol{\alpha}$) increases with Wi, this increase is almost completely driven by the mean shear. Indeed, for simple shear at the Wi values indicated (16, 20, and 28), the values of tr($\boldsymbol{\alpha}$) are 398, 560, and 877, respectively. The values at the wall for the edge states are only slightly larger than these. Furthermore, noting that the equilibrium magnitude of $\alpha_{yy} + \alpha_{zz}$ is $2b/(b+5) \approx 2$, we see that the polymer is essentially undeformed in y and z. Polymer stretching in these directions is the main cause of vortex suppression and DR in near-wall turbulence [24–26], and the lack thereof in the edge solution indicates why the edge structures are so weakly affected by viscoelasticity. The edge states are only barely three-dimensional and are thus almost completely unable to generate the exponential stretching of fluid elements required to strongly deform polymer chains. This very weak three-dimensionality is also seen in the lower-branch exact coherent states found by Wang *et al.* [27], which almost certainly also live on or near the laminar-turbulent boundary. Furthermore, these traveling waves have vanishing Reynolds shear stress in the limit of high Reynolds number—small Reynolds shear stress is a key feature of drag reduction and plays an important role in phenomenological models of it [11]. Based on the Wang *et al.* results and those here, it may be that the Reynolds shear stress vanishes at MDR as Re $\to \infty$.

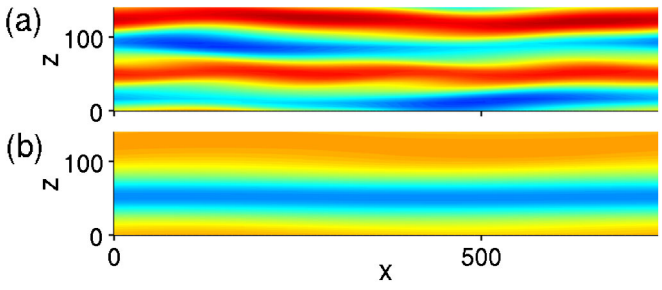

FIG. 3 (color online). Streamwise velocity [range 0.2 (blue)-0.7 (red)] on the xz plane at $y^+ = 25$ for (a) instant (I) and (b) instant (II) of Fig. 1.

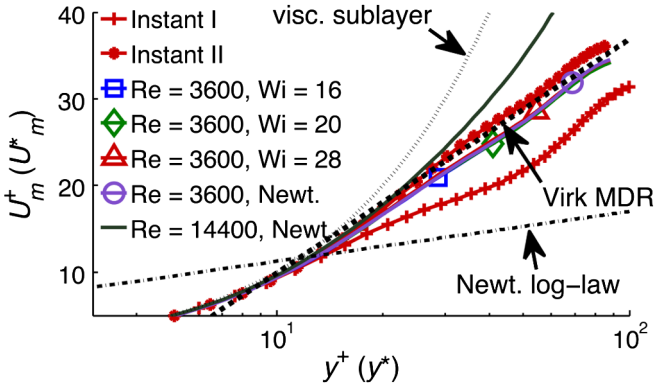

FIG. 4 (color online). Mean velocity profiles (half-channel). Lines with multiple markers are instantaneous profiles (for instants (I) and (II) on Fig. 1), in $*$ units; lines with single markers are time-average profiles, in $+$ units.

Discussion so far has focused on Re = 3600, where the turbulent flow structures are relatively simple. Figures 2(a) and 4 show results for a Newtonian edge state at Re = 14 400. Specifically, consider the mean velocity profile shown in Fig. 4. In contrast to the Re = 3600 result, the profile at Re = 14 400 remains close to the Virk asymptote up to $y^+ \approx 30$, but exceeds it at larger distances. This result indicates that at this Reynolds number the edge dynamics are even more weakly turbulent than the Virk MDR dynamics. This result is consistent with the bifurcation analysis study of Pringle *et al.* [28], which shows that as Re increases, a multitude of new traveling wave solutions come into existence. As new solutions arise, the position of the edge in state space can change discontinuously, so an invariant set that lies on the edge at a low Reynolds number may no longer be on the edge at higher Reynolds number. Much further work remains before the Reynolds number dependence of the laminar-turbulent boundary is understood.

The key qualitative conclusion from this study is that asymptotic trajectories on the laminar-turbulent boundary at low Reynolds number are insensitive to viscoelasticity—they are only weakly three-dimensional and are thus ineffective at stretching polymers. Furthermore, the mean velocity profile for the Newtonian edge state quantitatively agrees with the experimentally observed profile for polymer solutions at the maximum drag reduction asymptote. These conclusions present a solution to the long-standing question of why there is an upper limit for DR and why it is universal with respect to polymer properties. Conventional ''active'' turbulence generates substantial polymer stretching, which in turn acts to weaken the turbulence, driving the dynamics toward the laminar-turbulent boundary—hibernation intervals are excursions toward the edge (necessarily transient as edge states are saddles in state space), as evidenced by the strong similarity in flow structure between the two phenomena. From the present work we now see that the weakest form of self-sustaining turbulence, the edge state, is not affected by polymer, so we can also conclude that there is a region in the state space close to the laminar-turbulent boundary where turbulent motion is too weak to sufficiently stretch polymers and is thus insensitive to them. This region forms a band in the state space that is invariant to viscoelasticity, determining the upper limit of polymer-induced DR.

From a broader perspective, this work bridges two important areas, laminar-turbulent transition and drag reduction by polymers, which have generally been viewed as separate. In addition, if MDR is indeed closely connected to Newtonian flow states, as strongly indicated in this study and previous ones [4,5,9], achieving high levels of DR with flow control instead of polymer additives might be a realistic goal.

The authors thank Fabian Waleffe and Bruno Eckhardt for many helpful discussions. The code used here is based on ChannelFlow by John F. Gibson, who we gratefully acknowledge. This work is supported by grants from the NSF and through its support of MDG during his stay at the Institute for Mathematics and Its Applications, and by the AFOSR.

*Corresponding author.
graham@engr.wisc.edu

[1] P. S. Virk, AIChE J. **21**, 625 (1975).
[2] M. D. Graham, in *Rheology Reviews 2004*, edited by D. M. Binding and K. Walters (British Society of Rheology, Aberystwyth, UK, 2004) p. 143.
[3] C. M. White and M. G. Mungal, Annu. Rev. Fluid Mech. **40**, 235 (2008).
[4] L. Xi and M. D. Graham, Phys. Rev. Lett. **104**, 218301 (2010).
[5] L. Xi and M. D. Graham [J. Fluid Mech. (to be published)].
[6] C. M. White, V. S. R. Somandepalli, and M. G. Mungal, Exp. Fluids **36**, 62 (2004).
[7] K. D. Housiadas, A. N. Beris, and R. A. Handler, Phys. Fluids **17**, 035106 (2005).
[8] C. F. Li, R. Sureshkumar, and B. Khomami, J. Non-Newtonian Fluid Mech. **140**, 23 (2006).
[9] S. Tamano, M. D. Graham, and Y. Morinishi, J. Fluid Mech. **686**, 352 (2010); Y. Dubief, C. M. White, E. S. G. Shaqfeh, and V. E. Terrapon, Center for Turbulence Research Annual Research Briefs (2011).
[10] J. Jovanović, M. Pashtrapanska, B. Frohnapfel, F. Durst, J. Koskinen, and K. Koskinen, J. Fluids Eng. **128**, 118 (2006).
[11] R. Benzi, E. De Angelis, V. S. L'vov, and I. Procaccia, Phys. Rev. Lett. **95**, 194502 (2005); I. Procaccia, V. S. L'vov, and R. Benzi, Rev. Mod. Phys. **80**, 225 (2008).
[12] J. D. Skufca, J. A. Yorke, and B. Eckhardt, Phys. Rev. Lett. **96**, 174101 (2006).
[13] J. Vollmer, T. M. Schneider, and B. Eckhardt, New J. Phys. **11**, 013040 (2009).
[14] N. R. Lebovitz, Commun. Nonlinear Sci. Numer. Simul. **17**, 2095 (2012).
[15] B. Eckhardt, H. Faisst, A. Schmiegel, and T. M. Schneider, Phil. Trans. R. Soc. A **366**, 1297 (2008); B. Hof, J. Westerweel, T. M. Schneider, and B. Eckhardt, Nature (London) **443**, 59 (2006).
[16] S. Toh and T. Itano, J. Fluid Mech. **481**, 67 (2003).
[17] T. M. Schneider, B. Eckhardt, and J. A. Yorke, Phys. Rev. Lett. **99**, 034502 (2007).
[18] Y. Duguet, A. P. Willis, and R. R. Kerswell, J. Fluid Mech. **613**, 255 (2008).
[19] R. B. Bird, C. F. Curtis, R. C. Armstrong, and O. Hassager, *Dynamics of Polymeric Liquids* (John Wiley & Sons, Inc., New York, 1987), 2nd ed., Vol. 2.
[20] L. Xi and M. D. Graham, J. Fluid Mech. **647**, 421 (2010).
[21] M. D. Warholic, H. Massah, and T. J. Hanratty, Exp. Fluids **27**, 461 (1999).

[22] T. Min, H. Choi, and J. Y. Yoo, J. Fluid Mech. **492**, 91 (2003).
[23] P. K. Ptasinski, B. J. Boersma, F. T. M. Nieuwstadt, M. A. Hulsen, B. H. A. A. van den Brule, and J. C. R. Hunt, J. Fluid Mech. **490**, 251 (2003).
[24] Y. Dubief, V. E. Terrapon, C. M. White, E. S. G. Shaqfeh, P. Moin, and S. K. Lele, Flow Turbul. Combust. **74**, 311 (2005).
[25] W. Li and M. D. Graham, Phys. Fluids **19**, 083101 (2007).
[26] K. Kim, C. F. Li, R. Sureshkumar, S. Balachandar, and R. J. Adrian, J. Fluid Mech. **584**, 281 (2007).
[27] J. Wang, J. F. Gibson, and F. Waleffe, Phys. Rev. Lett. **98**, 204501 (2007).
[28] C. C. T. Pringle, Y. Duguet, and R. R. Kerswell, Phil. Trans. R. Soc. A **367**, 457 (2009).